ACS OMEGA

Article

Cite This: ACS Omega 2020, 5, 2541−2551

Time-Domain Terahertz Spectroscopy and Density Functional Theory Studies of Nitro/Nitrogen-Rich Aryl-Tetrazole Derivatives

Damarla Ganesh,[†,⊥] Elaprolu Narsimha Rao,[†,⊥] Mottamchetty Venkatesh,[†,§] Kommu Nagarjuna,[†] Ganapathy Vaitheeswaran,[†,‡] Akhila K. Sahoo,[†,∥] and Anil K. Chaudhary*[,†]

[†]Advanced Center of Research in High Energy Materials (ACRHEM), [‡]School of Physics, and [∥]School of Chemistry, University of Hyderabad, Prof. C. R. Rao Road, Gachibowli, Hyderabad 500 046, Telangana, India

[§]The Guo China-US Photonics Laboratory, State Key Laboratory of Applied Optics, Changchun Institute of Optics, Fine Mechanics and Physics, Chinese Academy of Sciences, Changchun 130033, China

ABSTRACT: The paper reports the time-domain THz spectroscopy studies of noncentrosymmetric energetic nitro/nitrogen-rich aryl-tetrazole high-energy molecules. The fingerprint spectra in the THz domain reveal the role of different functional groups attached to position "1" of the tetrazole moiety, which controls the energetic properties. These responses are deliberated through density functional theory (DFT) calculations. The synthesized aryl-tetrazoles exhibit high positive heat of formation (369−744 kJ/mol), high detonation velocities, and pressures (D_v: 7734−8298 m·s^{-1}; D_p: 24−28 GPa) in comparison to the noncentrosymmetric 2,4,6-trinitrotoluene (TNT). These compounds exhibit variation in the refractive indices and absorption between 0.1 and 2.2 THz range. The DFT studies at the molecular and single-crystal level (using plane wave pseudo potential method) endorse in detecting these bands (with ∼1% deviation). The calculated vibrational frequencies and linear optical properties are found to have good agreement with the experimental data in UV−visible and THz regions.

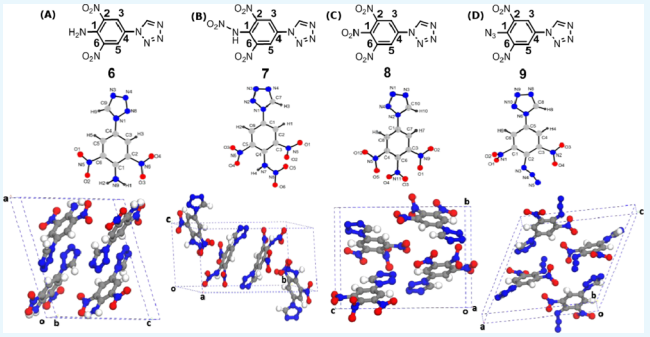

INTRODUCTION

The electromagnetic radiation between 0.1 and 3.0 THz range receives special attention in telecommunication industries because of broad band communication. In addition, it has the ability to pass through paper, leather, plastic, rubber, and different types of organic nonpolar packing materials including semiconductors, explosives, drugs, and biomolecules without ionizing the test sample. Therefore, THz-based spectroscopy and imaging are an effective means for detection of concealed objects and play a very significant role in home land security, defence, and medical fields. Because the THz spectrum lies between 100 and 5.0 cm^{-1} range which covers the weak vibrational frequency of organic molecules, the technique provides important information about the structural dynamics and intermolecular vibrations of high energy molecules (HEMs) and also helps to assign the periodicity of the materials through polymorphism and phase transition.[1−5]

In view of the importance of the time-domain THz spectroscopy technique and density functional theory (DFT)-based theoretical approach help us to study the structure−properties and correlation of HEMs.[17,18] Our group has also explored different types materials such as LT/SIGaAs-based photoconductive antenna and organic and semiconductor crystals for THz generation and its application in time-domain spectroscopy of HEMs.[19−22] Because tetrazole derivatives show superior energetic properties as compared to the other five-membered azole moieties because of high contents of nitrogen and higher value of positive heat of formation, their physical properties are comparable with premium explosives like Research department explosive (RDX) and 2,4,6-trinitrotoluene (TNT).[6−10,27,28] However, most of the reported tetrazole derivatives are very sensitive to impact and friction.[11−13] Pellizzeri et al.[35] reported the polymorphic characterization of 5(4-pyridyl)tetrazole using time-domain THz spectroscopy and solid-state DFT. A deliberation for the synthesis of nitro/nitroamino/azido-substituted aryl tetrazole derivatives, such as 2,6-dinitro-4-(1*H*-tetrazol-1-yl)aniline ($C_7H_5N_7O_4$) (6), *N*-(2,6-dinitro-4-(1*H*-tetrazol-1-yl)phenyl)nitramide ($C_7H_4N_8O_6$) (7), 1-(3,4,5-trinitrophenyl)-1*H*-tetrazole ($C_7H_3N_7O_6$) (8), and 1-(4-azido-3,5-dinitrophenyl)-1*H*-tetrazole ($C_7H_3N_9O_4$) (9) are recently reported because these compounds exhibit better energetic properties than TNT and are comparable to RDX. The important parameters are comprised in Table 1. It is interesting to see that all these reported compounds are crystalline in nature and can be used as an energetic plasticizer in rocket propulsion applications because of their good oxygen balance (OB %). For example, compounds "6", "7", "8", and "9" possess OB (%) of the order of

Received: December 3, 2018
Accepted: May 13, 2019
Published: February 7, 2020

DOI: 10.1021/acsomega.8b03383
ACS Omega 2020, 5, 2541−2551

Table 1. Energetic Properties of 6−9 Compounds[a]

compound	(ρ)	D_v	D_p
2,6-dinitro-4-(1*H*-tetrazol-1-yl)aniline (6)	1.75	7899	24.1
N-(2,6-dinitro-4-(1*H*-tetrazol-1-yl)phenyl) nitramide (7)	1.78	8208	28.0
1-(3,4,5-trinitrophenyl)-1*H*-tetrazole (8)	1.79	8298	28.4
1-(4-azido-3,5-dinitrophenyl)-1*H*-tetrazole (9)	1.66	7734	26.2
TNT	1.65	6881	19.5
RDX	1.80	8795	34.9

[a]Here ρ (in g·cm^{-3}), D_v (in m·s^{-1}), D_p (in GPa) are crystal density, detonation velocity and detonation pressure reported from ref 16.

−79.62, −54.02, −54.06, and −66.38%, respectively. In addition, their corresponding densities ρ (in g·cm^{-3}), high detonation velocities D_v (in m·s^{-1}) and detonation pressure D_p (in GPa) are shown in Table 1. We also compared the important chemical and physical parameters with well-known energetic plasticizer, that is, bis(2-fluoro-2,2-diniroethyl)formal (it possess OB % = −74.0%, D_v = 7500 m·s^{-1}, D_p = 25 GPa).[14] However, the functional group attached to position "1" of the molecule as shown in Figure 1 not only influences the energetic properties of the molecules but also is responsible for the transition of crystalline to the amorphous phase which is also reflected in terms of change in the refractive index and absorption coefficient. Moreover, all these aryl-tetrazole derivatives are noncentrosymmetric with space groups $P2_1/C$ and $P2_12_12_1$. Therefore, we intended to study the structure−property correlations of these molecules through experiments and theory. This will help us in examining the potential of terahertz generation, detection, and nonlinear optical (NLO) response. Here, we have discussed the THz time-domain, UV−visible spectroscopic studies of the energetic polynitro-arene-tetrazole derivatives.[15] The possible reasons behind the optical response through DFT calculations both at molecular and solid levels are also provided. The experimental crystal structures are shown in Figure 1, and the corresponding energetic properties are comprised in Table 1 for reference.

EXPERIMENTAL SETUP AND SAMPLE PREPARATION

The sample pellets of 12 mm diameter of weight 500 mg were prepared by mixing 100 mg of sample with 400 mg of Teflon [polytetrafluoroethylene (PTFE)] powder. Particle sizes are comparable with far infrared (FIR) wavelength which leads to scattering losses from the surface of the pellets. This can be minimized by mixing the compound and PTFE powder with ethanol solution and subsequently grounding with mortar to make a homogeneous mixture. The mixture was dried for half an hour before subjecting to press mills. The whole mixture was loaded into a die and pressed with 2 tons of hydraulic pressure. The diameter and thickness of pellets are 12 and 2mm, respectively. A pure Teflon pellet of identical size is also prepared for reference. Figure 2 shows the experimental layout

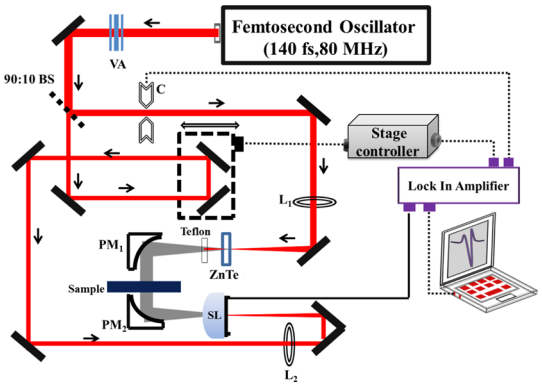

Figure 2. Schematic diagram of our terahertz time-domain spectroscopy experimental setup.

of THz generation and detection. A Ti:sapphire laser-tunable oscillator laser with pulse duration 140 fs at a repetition rate of 80 MHz (coherent chameleon ultra-II made) was used as a pumping source. Using a 90:10 beam splitter, the laser beam was split into a pump and probe. A transmitted pump beam is used for pumping the ZnTe crystal for terahertz generation. It is generated by the optical rectification process. A Teflon sheet was

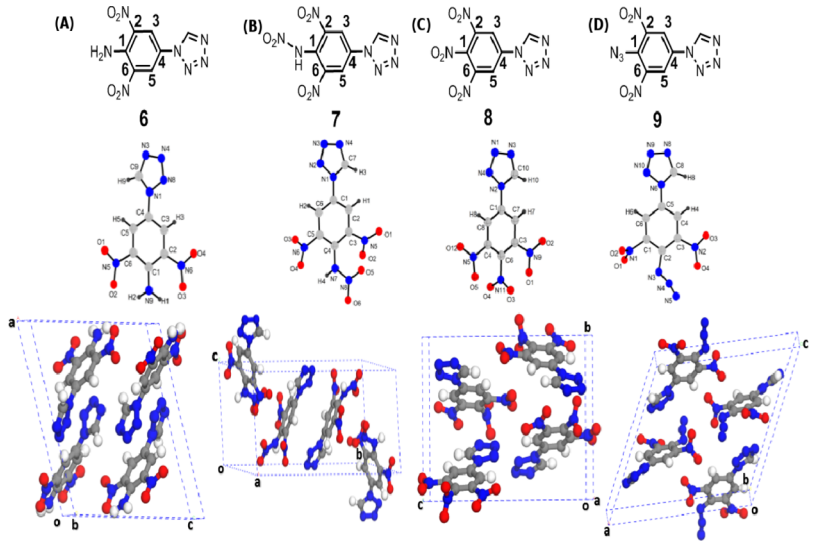

Figure 1. Molecular and experimental crystal structures[15] (from left to right) of (A) $C_7H_5N_7O_4$ (6), (B) $C_7H_4N_8O_6$ (7), (C) $C_7H_3N_7O_6$ (8), and (D) $C_7H_3N_9O_4$ (9). Here "*a*", "*b*", and "*c*" are lattice vectors.

DOI: 10.1021/acsomega.8b03383
ACS Omega 2020, 5, 2541−2551

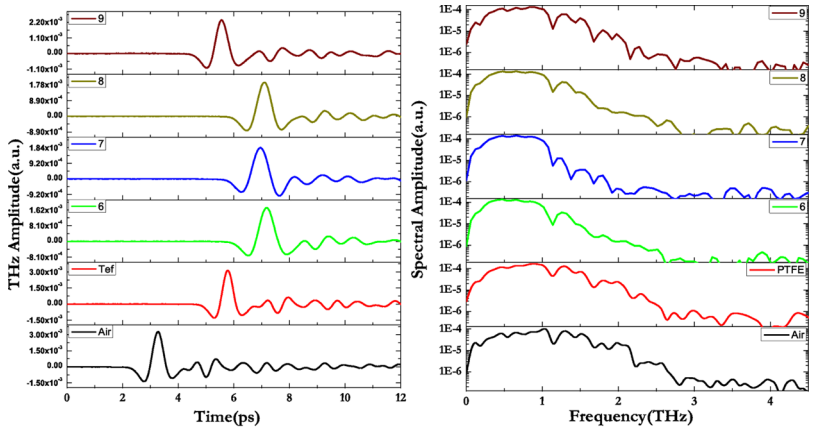

(a) a (b) b

Figure 3. (a)Time-domain THz spectra of tetrazole molecules, (b) corresponding frequency domain spectra.

used for filtering out the undesirable pump wavelength from terahertz. A half axis parabolic mirror is used to collimate and focus the generated THz radiation for detection using a photoconductive antenna (gap ≈ 5 μm, length ≈ 20 μm). In the detection arm, the reflected beam is passed through a linear translation stage and loosely focused on detecting antenna. The photoconductive antenna is connected to a low-noise current preamplifier which is fed to the lock-in amplifier (Stanford Research Systems, model no. SR830). A mechanical chopper operating at 1.5 kHz is used as a reference to the lock-in amplifier (Stanford Research Systems, model no. SR830). The data acquisition and motion control of delay stage are done by software using LabView program. All measurements were carried out at room temperature under ambient conditions. The THz temporal profile is measured by changing the delay of probe beam with respect to the THz pulse reaching to the antenna. Initially, the scan was done without any sample followed by pure Teflon pellet mounted in front of the antenna. The temporal data are converted to the frequency domain by performing fast Fourier transform (FFT). Material parameters like spectral transmittance, phase, and absorption coefficient are obtained from frequency domain data, whereas the refractive index can be obtained from both temporal and spectral data without using the Kramers–Kronig relation. Figure 3 shows terahertz temporal profile and corresponding FFT of air and Teflon pellet are shown in the inset.

Refractive index ($n(\omega)$) and absorption coefficient ($\alpha(\omega)$) were calculated from the FFT spectrum.[23] The intensity ratio of the transmitted radiation from the sample and reference provides the actual transmittance of the sample pellets and is given by eq 1

$$T = \frac{E_{\text{sample}}}{E_{\text{reference}}} \tag{1}$$

It is related to the complex refractive index $N = n + ik$, where the real part corresponds to the refractive index and the imaginary part is molar absorptivity. For measurement of the complex refractive index between 0.1 and 2.6 THz range, we have calculated the effective thickness of the sample distributed in the Teflon matrix using eq 2.

$$l = \frac{m}{\rho}\frac{4}{\pi D^2} \tag{2}$$

here, m = weight of the sample (100 mg), D = diameter of sample (12 mm), and ρ is density of the sample. Figure 2 shows the time-domain spectrum of explosive molecules. Because the pellets contain a mixture, the absorption coefficient (α) is calculated using eq 3.

$$\text{Absorption coefficient} = -\frac{1}{l}\ln\frac{T_{\text{m}}}{T_{\text{s}}} \tag{3}$$

where "l" is the effective thickness of the sample and T_{m} and T_{R} are the spectra of THz transmitted through material and reference samples, respectively. Because the particle sizes of both Teflon powder and sample are very small compared with the wavelength of radiation, one can neglect scattering losses. The refractive index is calculated using eq 4.

$$n = 1 + \frac{\delta\pi c}{2\pi\nu d} \tag{4}$$

where $\delta\pi$ is the phase difference between reference and sample, ν is frequency, d is thickness of pellet, and c is the velocity of light.

THEORETICAL METHODS

The solid-level theoretical calculations are performed with Cambridge Series of Total Energy (CASTEP) program,[29,30] whereas the molecular-level calculations are done with Gaussian-03 code. We have considered the experimental crystal structures reported by Kommu et al.[15] as input and optimized the systems using Broyden–Fletcher–Goldfarb–Shanno algorithm[31] with convergence thresholds for energy, force, stress, and maximum displacements as 5.0×10^{-6} (eV/atom), 0.01 eV/Å, 0.02 GPa, and 5.0×10^{-4} Å, respectively. The electronic Hamiltonian with the plane wave basis set with cutoff energy 550 eV, ultrasoft (US) pseudopotentials (for electron–ion interactions),[32] self-consistent field threshold 5.0×10^{-6} (eV/atom) with 3 × 5 × 3 Monkhorst–Pack[33] k-mesh (15 irreducible k-points) in the reciprocal space is used. Generalized gradient approximation (GGA), Perdew–Burke–Ernzerhof (PBE),[34] and dispersion correction Grimme (G06) scheme[36] are used to treat the strong and weak electron–electron interactions. The G06-optimized structure is used for linear optical property (absorption and refractive index spectra's) calculations. The zone centre vibrational properties (infrared (IR)-spectra) are calculated using density functional perturbation theory (DFPT)[38,39] approach by utilizing the norm conserving

DOI: 10.1021/acsomega.8b03383
ACS Omega 2020, 5, 2541−2551

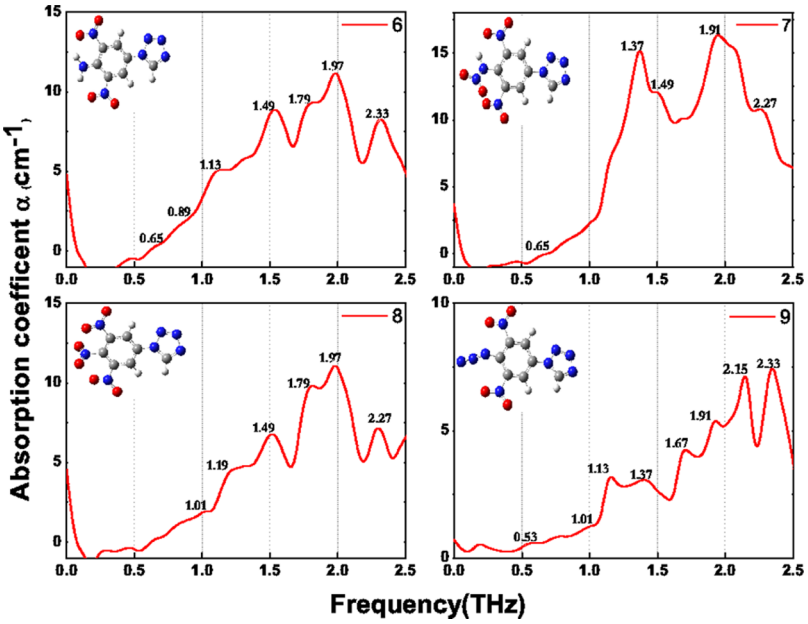

Figure 4. Experimental tera-hertz time-domain absorption spectra of 6, 7, 8, and 9. The calculated molecular level vibrational frequencies with Gaussian-03 are displayed as straight lines.

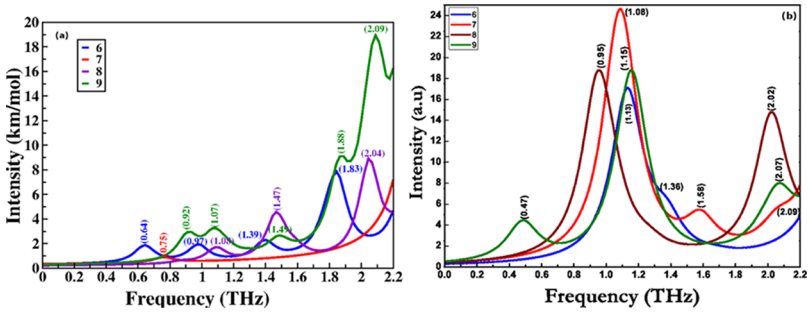

Figure 5. Calculated (a) single-molecule (b) single-crystal zone center vibrational (IR) spectra in 0.1−2.2 THz region of 6, 7, 8, and 9 using PBE + G06 dispersion-corrected method at the theoretical equilibrium structure.

pseudopotentials[40] with 830 eV cutoff energy. The valence electrons of the constituent atoms are considered as follows: H ($1s^1$), N($2s^2$ $2p^3$), C ($2s^2$ $2p^2$), O ($2s^2$ $2p^4$). The gas-phase single-molecule geometry optimizations and vibrational properties calculations are done using the B3LYP (Becke, 3-parameter, Lee−Yang−Parr) functional[41,42] with 6-311+G(d, p) polarized basis set as implemented in Gaussian-03.[24]

RESULTS AND DISCUSSION

Crystal Structure and Terahertz Time-Domain Response. All the chosen compounds ($C_7H_5N_7O_4$) (6), ($C_7H_4N_8O_6$) (7), ($C_7H_3N_7O_6$) (8), and ($C_7H_3N_9O_4$) (9) for the present study crystallize in noncentrosymmetric space groups with monoclinic symmetry except compound "8" which is orthorhombic.[15] These materials consist of z = 4 formula units/unit cell (i.e., compound "6"—92; compound "7"—100; compound "8"—92; and compound "9"—92 atoms/unit cell). Moreover, all of the atoms of compounds 6, 7, and 9 are located at "4e" atomic Wyckoff sites, whereas in compound "8", atoms are occupying "4a" Wyckoff site with full occupancy. Because of the change in the explosive functional groups (i.e. NH_2, NH−NO_2, NO_2, N_3) of these tetrazole derivatives, the lattice vectors show an increment in the following order: lattice vector "a": from compound "8" → "7" → "6" → "9"; lattice vector "b": from compound "9" → "6" → "8" → "7"; lattice vector "c": from compound "7" → "6" → "9" → "8"; and lattice angle β: from compound "8" → "7" → "6" → "9". From the experimental crystal structure, it is clear that all the studied compounds are naturally layered. The corresponding layers of compounds 6, 7, 8, and 9 are spread over xz, xy, yz, and xz planes, and the adjacent layers are stacked along x, y, z, and x directions. The change in the chemical composition and symmetry resulted in huge difference in their explosive nature (see Table 1) and stability. Moreover, the increase in the nitrogen and oxygen percentage in the studied compounds will definitely lead to change in their polarization. Hence, the noncentrosymmetric nature and change in the number of electrons strongly motivated us to investigate their terahertz optical responses, which are believed to be useful for their detection and nonlinear applications. The same was carried out using a time-domain terahertz spectroscopy setup.

The corresponding absorption spectra results of the studied compounds are shown in Figure 4. It is clear from the figure that (1) all of the compounds start absorbing radiation from 0.5 THz and high intensity absorption peaks are found between 1.0 and 2.5 THz range. (2) The studied materials show absorption in 0.5−2.5 THz energy window as follows: for compound "6"—0.65, 0.89, 1.13, 1.49, 1.79, 1.97, 2.33 THz; for compound "7"—0.65, 1.37, 1.49, 1.91, 2.27 THz; for compound "8"—1.01, 1.19,

DOI: 10.1021/acsomega.8b03383
ACS Omega 2020, 5, 2541−2551

Table 2. Calculated Ground-State Lattice Vectors (a and c, in Å), Volume (V, in Å^3) of 6, 7, 8, and 9 Using PBE and Dispersion-Corrected PBE + G06 along with Experimental Data[15]

symmetry	compound	parameter	PBE	PBE + G06	experiment
$P2_1/C$	6	a	14.593	12.941	12.780
(z = 4)		b	7.278	7.067	7.1353
(monoclinic)		c	11.910	10.754	11.0435
		V	1144.690	934.862	948.6
		β	115.198	108.109	109.625
$P2_1/C$	7	a	8.233	7.871	7.9223
(z = 4)		b	19.821	18.690	18.5920
(monoclinic)		c	8.105	7.642	7.5610
		V	1286.70	1109.11	1100.77
		β	103.388	99.442	98.730
$P2_12_12_1$	8	a	8.317	7.528	7.6268
(z = 4)		b	11.086	10.518	10.5375
(orthorhombic)		c	14.154	13.654	13.5924
		V	1305.22	1081.33	1040.25
$P2_1/C$	9	a	14.724	14.249	13.9435
(z = 4)		b	7.104	6.872	6.9570
(monoclinic)		c	14.093	12.825	12.8193
		V	1367.89	1125.51	1104.4
		β	111.906	116.355	117.363

1.49, 1.79, 1.97, 2.27 THz; and for compound "9"—0.53, 1.01, 1.13, 1.37, 1.67, 1.91, 2.15, 2.33 THz. (3) Among these, compound "7" shows highest intensity peaks and hence is more polarizable, whereas compound "9" shows well-defined absorption peaks and hence is relatively more sensitive and easy to detect even at lower energies. (4) Moreover, the detection limit of the studied tetrazole compounds got increased from NH−NO_2 → NH_2 → NO_2 → N_3 explosive functional groups. These unique absorption spectra of studied compounds are considered to be their fingerprint spectra's in the terahertz domain. To understand these absorption peak frequency and intensity differences more clearly, we extended our focus toward the vibrational mode analysis using DFT calculations both at molecular and solid levels.

In the first step, we performed the molecular vibrational spectra calculations by using B3LYP/6-311+G(d,p) polarized basis set as implemented in Gaussian-03.[24] We have considered the experimental single-crystal X-ray diffraction structure as our input. The obtained frequencies do not show any imaginary part, which confirm the dynamical stability of all the studied compounds, and the corresponding results are plotted in Figure 5. The FIR absorption peaks of studied tetrazole molecules between 0.1 and 2.2 THz frequency window are observed at the following frequencies (as shown in Figure 5): for compound "6"—1.13, 1.36 THz; for compound "7"—1.08, 1.58, 2.09 THz; for compound "8"—0.95, 2.02 THz; and for compound "9"—0.47, 1.15, 2.07 THz. The obtained results show considerable deviation with respect to the experimentally measured frequencies. However, it is known that the vibrational spectrum in the THz range depends primarily on the structure of molecules and their intra- and intermolecular interaction. The weak interaction of molecules and intermolecular force result in the collective vibration mode under the THz range frequency. The low-frequency vibration in the THz range normally comes from the deformation, torsion, and bending of two or more molecules. As we performed the DFT calculations at the single-molecule level, the obtained vibrational spectrum in the 0.2−2.2 THz region can be attributed to the intramolecule vibrations alone. The preliminary mode analysis informs that the absorption peak of compound "6" located at 1.13 THz is attributed to torsional rotation of tetrazole moieties, and other two frequencies are due to wagging of NO_2 groups attached to the ring. The peak of compound "7" at 1.08 THz is attributed to torsional rotation of the tetrazole moiety. Similarly, the reduction in the first absorption peak (red shift) of compounds "7"(1.08), "8"(0.95), "9"(0.47) when compared to compound 6(1.13) are due to increase of the additional nitro group reduced mass of the molecule. The mode at 2.02 THz of compound "8" is attributed to the rotation of twist of NO_2, and the calculated low-frequency 0.95 THz mode is not clearly observed in the experimental spectrum, which could be due to the scattering losses. In case of compound "9", mode at 0.47 THz is observed due to collective rotation twists of all attached azide groups to the ring. Torsional rotation of the tetrazole moiety was observed at 1.15 THz. A torsional rotation of all functional groups except for tetrazole was observed theoretically at 2.07 THz. The difference in the intensity profiles of the studied molecules (Figure 5b) indicates the increment in the polarizability from compounds "6" → "9" → "8" → "7", which is contradicting with the experimental observations. However, the observed discrepancy between experimental and theoretical vibrational frequencies could be due to the omission of the effects from intermolecular interaction and temperature. Hence, we turned our attention to the solid-state-level DFT calculations of the present compounds of interest to incorporate the role of intermolecular interactions.

Initially, we optimized the experimental layered non-centrosymmetric crystal structures[15] using the GGA-PBE exchange correlation functional[34] as implemented in CASTEP.[29,30] The calculated ground-state lattice vectors, angles, and volumes along with experimental data are shown in Table 2. The obtained results show considerable deviation as compared to the experimental data and are as follows: for compound "6" → a(14.1%) > c(7.8%) > b(2.0%); for compound "7" → c(7.1%) > b(6.6%) > a(3.9%); for compound "8" → a(9.0%) > b(5.2%) > c(4.1%); and for compound "9" → c(9.7%) > a(5.5%) > b(2.1%). The crystals volume and crystallographic angles deviations are as follows: V: for compound "8" (25.4%) > "9"

DOI: 10.1021/acsomega.8b03383
ACS Omega 2020, 5, 2541−2551

Table 3. Calculated Zone-Center Low-Frequency Vibrational Modes (in cm^{-1}) of $C_7H_5N_7O_4$) (6), ($C_7H_4N_8O_6$) (7), ($C_7H_3N_7O_6$) (8), and ($C_7H_3N_9O_4$) (9)[a]

compound	exp	mode	frequency	symmetry	compound	exp	mode	frequency	symmetry
6		M14	66.64	Bg(R)	7		M06	25.36(21.68)	Bg(I)
		M13	62.05(65.71)	Au(I)			M05	24.29	Au(R)
		M12	61.61(59.70)	Au(I)			M04	13.08	Ag(R)
		M11	59.42(—)	Bu(I)					
		M10	55.27	Ag(R)					
	65.71	M09	48.52	Bg(R)					
	59.70	M08	46.47(49.70)	Bu(I)					
	49.70	M07	41.37	Ag(R)		63.71			
	37.69	M06	37.03	Bg(R)		49.70			
	29.68	M05	32.60(29.68)	Bu(I)		45.69			
	21.68	M04	21.37(21.68)	Au(I)		21.68			
8					9		M24	73.32	Bg(R)
							M23	72.90(71.71)	Au(I)
							M22	70.69	Bg(R)
		M21	73.23	A(R)			M21	70.15	Ag(R)
		M20	69.94(—)	B3(I + R)			M20	68.41(—)	Bu(I)
		M19	69.29	A(R)			M19	67.47(—)	Au(I)
		M18	68.05(—)	B1(I + R)			M18	63.90(63.71)	Au(I)
		M17	66.70(65.71)	B2(I + R)			M17	63.58	Ag(R)
		M16	62.07(—)	B3(I + R)			M16	56.89	Bg(R)
		M15	61.68(59.70)	A(R)			M15	52.97(55.70)	Au(I)
		M14	51.90(—)	B3(I + R)			M14	48.94(45.69)	Bu(I)
		M13	49.52(49.70)	B2(I + R)			M13	47.91	Ag(R)
		M12	47.28(—)	B1(I + R)			M12	46.24	Ag(R)
		M11	43.05(—)	B2(I + R)			M11	46.23	Bg(R)
		M10	39.06(39.69)	B1(I + R)		71.71	M10	41.42	Bg(R)
		M09	38.47	A(R)		63.71	M09	39.78(—)	Au(I)
	65.71	M08	35.90(—)	B2(I + R)		55.70	M08	37.28	Ag(R)
	59.70	M07	33.98(33.68)	B1(I + R)		45.69	M07	36.36(—)	Bu(I)
	49.70	M06	30.44	A(R)		37.69	M06	32.79	Ag(R)
	39.69	M05	29.73(—)	B3(I + R)		33.68	M05	31.65	Bg(R)
	33.68	M04	20.90	A(R)		17.67	M04	29.12(—)	Au(I)

[a]Here, IR active modes are denoted as "I", Raman active modes are denoted as "R", and IR + Raman active modes are denoted as "I + R".

(23.8%) > "6" (20.6%) > "7" (16.8%) and β: for compound "6" (5.0%) > "7" (4.7%) > "9" (4.6%); these results also reveal that the intermolecular interactions are dominant in the studied layered compounds as follows: for compound "6" (in xz plane) > "9" (in zx plane) > "8" (in xy plane) > "7" (in zx plane). This can be attributed to the difference in the arrangement of molecules in corresponding unit cells. As the vibrational properties are very sensitive to the lattice vectors, it is important to optimize the crystal's structure to a better accuracy by including various interatomic interactions.[35,48] Hence, to capture the weak interlayer nonbonded interactions [van der Waals (vdW), hydrogen bond], we optimized all the crystal structures with the dispersion-corrected Grimme functional, that is, PBE + G06.[36] The obtained results show very good agreement with the experimental data, and the deviations of all of the obtained lattice vectors, volumes, and β values are around ~1% (see Table 2). Hence, the G06 optimization results confirm the crucial role of weak nonbonded interactions for finding the optimized structures. We have used these (G06) structures for our further vibrational property calculations which are very sensitive to the lattice vectors.

We have calculated the zone centre vibrational frequencies of all the compounds using DFPT approach. All of the required mode assignments from 0.1 to 2.2 THz are done, and the corresponding results are shown in Table 3. The compounds 6, 7, and 9 are isostructural and crystallized in the same point group with $C_{2h}(2/m)$ symmetry with $z = 4$ formula units (98 atoms/unit cell) except for compound "8" which is getting crystallized in $D_2(222)$ point group symmetry with 100 atoms/unit cell. Hence, there will be 276 − 3 = 273 vibrational modes for 6, 7, and 9 and 300 − 3 = 297 modes for compound "8". The group theory[37] representation for these acoustic (appear due to in-phase moment of atoms) and optical (appear due to out of phase moment of atoms) modes will be as follows

$$\Gamma_{acoustic}(6, 9) = A_u \oplus 2B_u$$

$$\Gamma_{optic}(6, 9) = 69A_g \oplus 68A_u \oplus 69B_g \oplus 67B_u$$

$$\Gamma_{acoustic}(7) = A_u \oplus 2B_u$$

$$\Gamma_{optic}(7) = 75A_g \oplus 74A_u \oplus 75B_g \oplus 73B_u$$

$$\Gamma_{acoustic}(8) = B_1 \oplus B_2 \oplus B_3$$

$$\Gamma_{optic}(8) = 69A_1 \oplus 68B_1 \oplus 68B_2 \oplus 68B_3$$

The calculated optical vibrational modes (273, 297) of the compounds are in good agreement with group theory representations. Among the 273 optical modes of compounds "6" and "9", 135 ($68A_u \oplus 67B_u$) are found to be IR (I) active and 138 modes ($68A_u \oplus 67B_u$) are found to be Raman (R) active. In

DOI: 10.1021/acsomega.8b03383
ACS Omega 2020, 5, 2541−2551

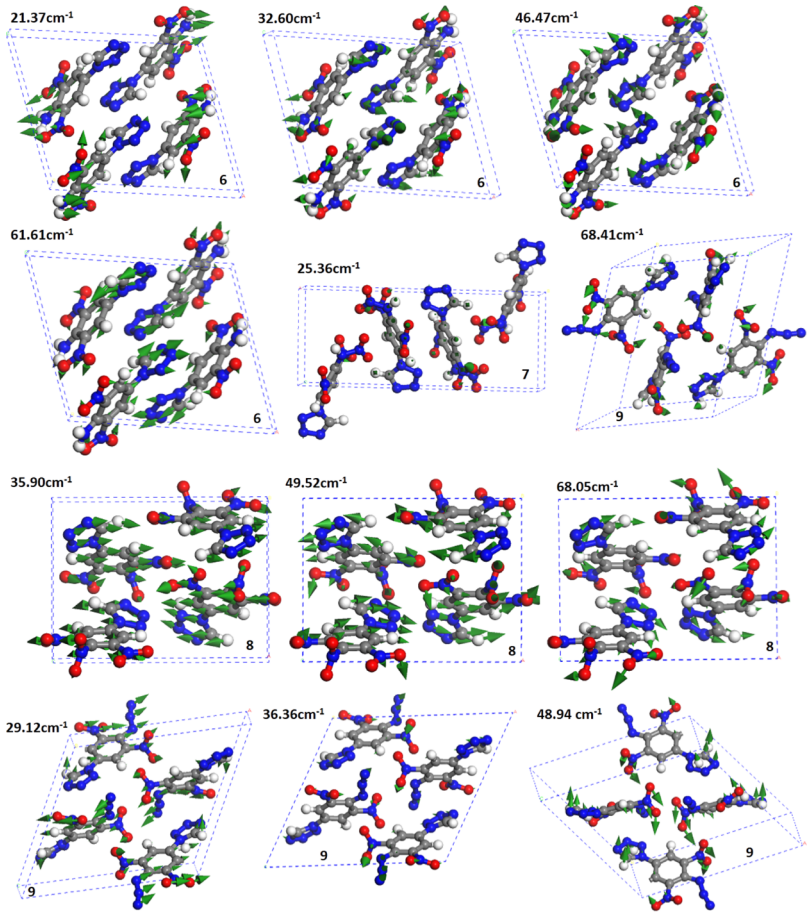

Figure 6. Few snapshot images of calculated vibrational frequencies (in cm^{-1}) at the solid level using PBE + G06.

case of compound "7", out of 297 optical modes, 147 modes ($74A_u \oplus 73B_u$) are found to be IR active and 150 modes ($75A_g \oplus 75B_g$) are Raman active. Interestingly, for compound "8", out of 273 optical modes, $69A_1$ modes are found to be purely Raman active and 204 modes ($68B_1 \oplus 68B_2 \oplus 68B_3$) are found to be both IR + Raman (I + R) active. Hence, we conclude that compound "8" is highly polarizable (more optically active) among the studied compounds. Because our current focus is on the terahertz response (0.1−2.2 THz range), mode assignments are done for these frequencies and the results are shown in Table 3. The corresponding vibrational spectra (IR) in 0.1−2.2 THz range is plotted in Figure 5. The snapshots of few vibrational modes are given in Figure 6 for future reference.

The mode assignment analysis reveals that the obtained frequencies of all the compounds between 0.1 and 2.2 THz range are mainly arising due to complete lattice translation associated with NO_2 groups and N_3 asymmetric stretching (see Figure 6), because of which asymmetric stretching in Tetrazole ring and trinitrobenzene has been observed. Few of the experimentally observed modes are well matched with the calculated symmetry-based IR frequencies (see Table 3). The main possible reasons for the observed discrepancies between theory and experimental frequencies and different broadening of the modes could be due to different scattering and temperature effects. Further, we have compared the experimental, solid-phase vibrational frequencies shown in Table 3 with the molecular phase. The results clearly indicate that most of the solid-level calculations match with the experimentally observed frequencies. The observed shift between the molecular-level and solid-level vibrational frequencies clearly indicates the dominant role of weak intermolecular, interlayer interactions via vdW and hydrogen bonding. To compare the intensity differences of the calculated frequencies, we have plotted the IR spectra in Figure 5. It is clear from the figure that intensities of the observed frequencies are dominant in the following order: compound "9" > "8" > "6" > "7". Hence, we can conclude that because of the different charge transfer mechanism of the azide group in the low-energy region, compound "9" is showing high peak intensity (polarizability) and hence is optically more sensitive. Similarly, in compound "8", because of the presence of an extra NO_2 group, electrons associated with all I + R active modes, it is showing next high polarizability. In case of compound "7", because of the presence of a strong N−N bond, we could observe only one peak in the studied terahertz range with lowest intensity among the studied compounds. However, compound "6" has weak C−N and H−N bonds because of which we are getting a good number of vibrational modes in the low energy region (<2.2 THz). Overall, we can conclude that because of the different charge transfer mechanisms, compound "9" possesses high optical sensitive (therefore unstable) nature, whereas compound "7" shows low optical sensitivity (highly stable) among the studied compounds. Other compounds show similar optical sensitivity in the studied region. In conclusion, it is easy to detect compound "8" and is optically stable than other studied noncentrosymmetric compounds. Hence, it may find possible applications in nonlinear optical domain also. Therefore, we further extended our attention to investigate the refractive index and birefringence of these compounds in the 0.1−2.2 THz range

DOI: 10.1021/acsomega.8b03383
ACS Omega 2020, 5, 2541−2551

which is a crucial parameter for obtaining proper phase matching in any nonlinear optical applications.

UV−Visible Response, Refractive Index, and Birefringence. The nitro/nitrogen-rich aryl-tetrazoles crystallize in the noncentrosymmetric space group, and it is very important to know the role of electronic contributions in the optical properties such as absorption, band gap, refractive index, and birefringence in the optical region of interest. Moreover, the THz-based study is meant for detection of explosives without ionizing the sample. Initially, we measured the absorption spectra of compounds using the UV/visible/NIR spectrometer (model: Cary 5000 with UMA attachment), and obtained results are compared with the theoretically calculated absorption spectra in [0 0 1] direction using the PBE-GO6 equilibrium structure as shown in Figure 7. The experimental results confirm

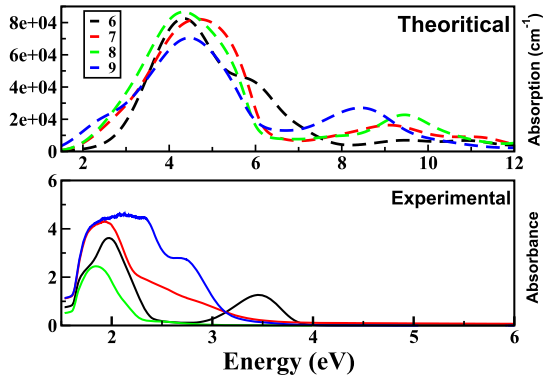

Figure 7. Experimental UV−visible absorption spectra of 6, 7, 8, and 9 compounds plotted along with the absorption spectra obtained at PBE + G06 equilibrium structure.

that compound "6" possesses a sharp absorption peak around 480 nm (2.58 eV), whereas absorption bands of other compounds such as "7", "8", and "9"are located at 450 nm (2.75 eV), 350 nm (3.54 eV), and 410 nm (3.02 eV), respectively. However, sharp absorption peaks for compounds "7", "8", and "9" are observed at 320 nm (3.87 eV), 280 nm (4.42 eV), and 475 nm (2.61 eV). This broadening may be attributed to the phonon contribution in optical transition (i.e., due to indirect band gap). However, the theoretically obtained absorption spectra show that sharp absorption peaks for compounds "6", "7", "8", "9" are located at 1.3, 1.2, 1.2, and 1.0 to 2.5 eV, respectively. The broadening of the absorption peak of compound "9" is attributed to the indirect band gap. Finally, it is clear from the experimental and theoretical results that the studied compounds possess a strong absorption band in the near-IR and THz region. Further, we have also calculated the frequency-dependent complex refractive index between 0.1 and 2.2 THz using eq 4. Etalon effects caused due to internal reflection were ineffective since we have not taken into account while calculating FFT. First, we have calculated the refractive index of Teflon by taking air as the reference.[25,26] Figure 3 shows the refractive index of Teflon between 0.1 and 2.2 THz range, and the value is 1.4 which is in good agreement with the literature values. Similarly, we calculated the average refractive index for compounds 6, 7, 8, and 9 (see Figure 8) and the obtained corresponding values are 1.65, 1.71, 1.72, and 1.81, respectively. We further verified these calculations by comparing with DFT results (see Figure 9). The calculations are done with great accuracy using US pseudopotentials, 380.0 eV energy

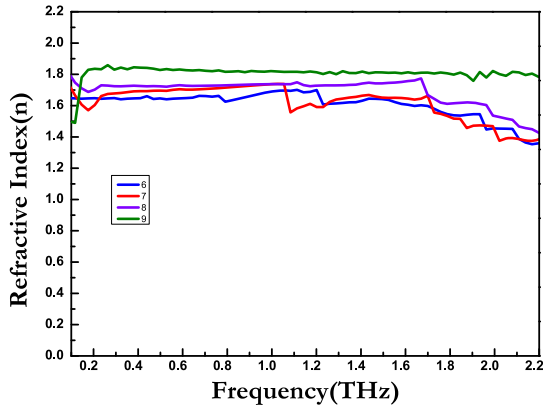

Figure 8. Experimental refractive index spectra comparison between 0 and 2.2 THz range of $C_7H_5N_7O_4$ (6), ($C_7H_4N_8O_6$) (7), ($C_7H_3N_7O_6$) (8), and ($C_7H_3N_9O_4$) (9).

cutoff, and 3 × 5 × 3 *k*-grid. As the chosen compounds crystallized in asymmetric space groups (monoclinic, orthorhombic), we could get different values of n_x, n_y, and n_z curves. All of the obtained results (experiment, DFT) within 0.1−2.2 THz energy window show reasonable agreement (Table 4), and the same are plotted in Figure 8. Moreover, the dispersion and intensity of the absorption curves are found to show considerable variation because of the change in the explosive functional group at position "1" on the tetrazole moiety. The theoretical difference in n_x, n_y, and n_z curves of studied compounds clearly indicate that all the compounds possess large optical anisotropy. Further, the theoretically calculated (time-independent DFT) absorption spectra shows considerable blue shift with respect to the experimental UV−visible spectra of the studied explosives, which is obvious due to the omission of local field effects and exciton effects in the present DFT calculations, and these deviations can be addressed properly by including the excitonic effects through time-dependent DFT calculations.[44]

The results in Figure 8 and Table 4 also confirm that the calculated average static refractive index ($(n = n_x + n_y + n_z)/3$) values of all the compounds are relatively good in agreement with the experimentally observed values. Normally, for monoclinic NLO crystals, the refractive indices show either $n_x > n_y > n_z$ (negative biaxial) or $n_z > n_y > n_x$ (positive biaxial) trend.[43] However, the results from Table 4 show the trend for compound "6": $n_y > n_z > n_x$, for compound "7": $n_z > n_x > n_y$, for compound "8": $n_z > n_x > n_y$, and for compound "9": $n_y > n_z > n_x$. These differences in the actual and obtained refractive indices can be attributed to the role of excitonic effects,[44] which are not accounted in the present study. For preliminary understanding, the birefringence (Δn) values of 6, 7, 8, and 9 compounds are calculated by taking the difference between the maximum value of refractive index to the minimum value from Table 4. The corresponding results show the following increment order: Δn (6) > Δn (8) > Δn (7) > Δn (9). Moreover, these values except for that of compound 9 are found to be closer to the well-known nonlinear crystal DAST (0.39, 0.55, and 0.64)[45] and higher than recently reported carbonate fluoride crystals $ABCO_3F$ (A = K, Rb, Cs; B = Ca, Sr, Pb) (Δn around 0.1056, 0.0887, 0.0921, 0.0966) crystal birefringence values,[46−49] which clearly indicates that the studied noncentrosymmetric explosive compounds may possess good phase matching applications in visible and near-IR regions. Further analyses on frequency-dependent second-harmonic response of these compounds will be useful in phase

DOI: 10.1021/acsomega.8b03383
ACS Omega 2020, 5, 2541−2551

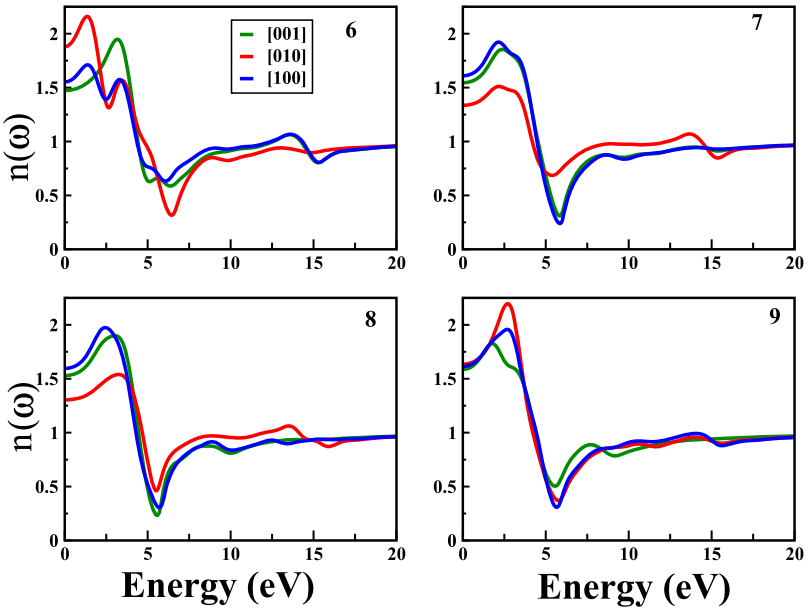

Figure 9. Theoretically obtained refractive index spectra (along *x*, *y*, *z* directions) of $C_7H_5N_7O_4$ (6), $C_7H_4N_8O_6$ (7), $C_7H_3N_7O_6$ (8), and $C_7H_3N_9O_4$ (9) at the PBE + G06 level.

Table 4. Experimental and DFT Calculated Refractive Indices (n) along [100], [010], and [001] Crystallographic Directions and Birefringence Values of 6, 7, 8, and 9

compound	n_x	n_y	n_z	Δn ($n_{max} - n_{min}$)	$n_{average}$	$n_{experiment}$
6	1.474	1.886	1.555	0.412(0.331)	1.63	1.65
7	1.546	1.337	1.611	0.274(0.065)	1.49	1.71
8	1.530	1.304	1.596	0.292(0.066)	1.47	1.72
9	1.589	1.635	1.616	0.046(0.019)	1.61	1.81

transition, sensitivity correlation studies, and designing new organic nonlinear optical materials in near future.

CONCLUSIONS

In summary, we have studied the linear and nonlinear optical properties of newly synthesized tetrazole molecules using time-domain terahertz spectroscopy, UV−visible−NIR spectroscopy, and DFT. We have also ascertained the absorption coefficients and refractive index between 0.1 and 2.2 THz range. In addition, we have performed single-molecule and single-crystal level DFT calculations. The obtained structural optimization results confirm the importance of nonbonded (vdW) interactions. The theoretically calculated zone center vibrational frequencies at the solid level are found to be good in agreement with the experimentally observed THz absorption bands. However, the single-molecule vibrational frequency-based results can be improvised by the incorporation of intermolecular, interlayer interactions. We have also explained the optical sensitivity correlations using vibrational frequencies. The electronic absorption, refractive index, and birefringence studies reveal the feasibility of phase-matched nonlinear optical frequency mixing device in the single-crystal form. The study also provides a good reference for growing organic nonlinear optical materials. We strongly believe that our present experimental and theoretical investigations on the studied explosives will open a new channel to design stable high-energy optical materials which may be used for different types of defence (detection purposes) and optical device applications.

AUTHOR INFORMATION

Corresponding Author

*E-mail: akcphys@gmail.com, anilphys@yahoo.com. Phone: 91 40 23138807.

ORCID

Ganapathy Vaitheeswaran: 0000-0002-2320-7667
Akhila K. Sahoo: 0000-0001-5570-4759
Anil K. Chaudhary: 0000-0003-1793-9930

Author Contributions

⊥Equal contribution.

Notes

The authors declare no competing financial interest.

ACKNOWLEDGMENTS

All the authors would like to thank DRDO, Ministry of Defence Govt. of India through ACRHEM under grant no. DRDO/18/1801/2016/01038:ARHEM-Phase-III for financial support. G.V. and E.N.R. would also like to acknowledge CMSD, University of Hyderabad, for providing computational facilities.

REFERENCES

(1) Tonouchi, M. Cutting-Edge Terahertz Technology. *Nat. Photonics* **2007**, *1*, 97−105.

(2) Davies, A. G.; Burnett, A. D.; Fan, W.; Linfield, E. H.; Cunningham, J. E. Terahertz Spectroscopy of Explosives and Drugs. *Mater. Today* **2008**, *11*, 18−26.

(3) Shen, Y. C.; Lo, T.; Taday, P. F.; Cole, B. E.; Tribe, W. R.; Kemp, M. C. Detection and Identification of Explosives Using Terahertz Pulsed Spectroscopic Imaging. *Appl. Phys. Lett.* **2005**, *86*, 241116.

DOI: 10.1021/acsomega.8b03383
ACS Omega 2020, 5, 2541−2551

(4) Parrott, E. P. J.; Fischer, B. M.; Gladden, L. F.; Jepsen, P. U.; Zeitler, J. A. Terahertz Spectroscopy of Crystalline and Non-Crystalline Solids. In *Terahertz Spectroscopy and Imaging*; Springer Series in Optical Sciences, 2013; Vol. *171*, pp 191−227.
(5) Brown, K. E.; Greenfield, M. T.; McGrane, S. D.; Moore, D. S. Advances in explosives analysis-part II: photon and neutron methods. *Anal. Bioanal. Chem.* **2016**, *408*, 49−65.
(6) Heppekausen, J.; Klapötke, T. M.; Sproll, S. M. Synthesis of Functionalized Tetrazenes as Energetic Compounds. *J. Org. Chem.* **2009**, *74*, 2460−2466.
(7) Kommu, N.; Ghule, V. D.; Kumar, A. S.; Sahoo, A. K. Triazole-Substituted Nitroarene Derivatives: Synthesis, Characterization, and Energetic Studies. *Chem.—Asian J.* **2014**, *9*, 166−178.
(8) Kumar, A. S.; Kommu, N.; Ghule, V. D.; Sahoo, A. K. Synthesis of trifluoromethyl-substituted N-aryl-poly-1,2,3-triazole derivatives. *J. Mater. Chem. A* **2014**, *2*, 7917−7926.
(9) Kommu, N.; Kumar, A. S.; Raveendra, J.; Ghule, V. D.; Sahoo, A. K. Synthesis, Characterization, and Energetic Studies of Polynitro Aryl-1,2,3-2 H-Triazoles. *Asian J. Org. Chem.* **2016**, *5*, 138−146.
(10) Kumar, A. S.; Ghule, V. D.; Subrahmanyam, S.; Sahoo, A. K. Synthesis of Thermally Stable Energetic 1,2,3-Triazole Derivatives. *Chem.—Eur. J.* **2013**, *19*, 509−518.
(11) Tang, Y.; Yang, H.; Wu, B.; Ju, X.; Lu, C.; Cheng, G. Synthesis and Characterization of a Stable, Catenated N11Energetic Salt. *Angew. Chem., Int. Ed.* **2013**, *52*, 4875−4877.
(12) Klapötke, T. M.; Piercey, D. G.; Stierstorfer, J. Amination of Energetic Anions: High-Performing Energetic Materials. *Dalton Trans.* **2012**, *41*, 9451−9459.
(13) Joo, Y.-H.; Shreeve, J. n. M. Nitroimino-Tetrazolates and Oxy-Nitroimino-Tetrazolates. *J. Am. Chem. Soc.* **2010**, *132*, 15081−15090.
(14) DeLuca, L. T.; Shimada, T.; Sinditskii, V. P.; Calabro, M. *Chemical Rocket Propulsion: A Comprehensive Survey of Energetic Materials*; Springer International Publishing: Switzerland, 2017; Vol. *2017*, pp 165−187.
(15) Kommu, N.; Balaraju, M.; Ghule, V. D.; Sahoo, A. K. Synthetic Manifestation of Nitro Substituted Tetrazole-N-(Hetero)Aryl Derivatives and Energetic Studies. *J. Mater. Chem. A* **2017**, *5*, 7366−7371.
(16) Sućeska, M. Calculation of Detonation Parameters by EXPLO5 Computer Program. *Mater. Sci. Forum* **2004**, *465*−*466*, 325−330.
(17) Venkataramudu, U.; Sahoo, C.; Leelashree, S.; Venkatesh, M.; Ganesh, D.; Naraharisetty, S. R. G.; Chaudhary, A. K.; Srinath, S.; Chandrasekar, R. Terahertz Radiation and Second-Harmonic Generation from a Single-Component Polar Organic Ferroelectric Crystal. *J. Mater. Chem. C* **2018**, *6*, 9330−9335.
(18) Narsimha Rao, E.; Vaitheeswaran, G. Structure-Property Correlation Studies of Potassium 4,4′-Bis(dinitromethyl)-3,3′-azofurazanate: A Noncentrosymmetric Primary Explosive. *J. Phys. Chem. C* **2019**, *123*, 10034.
(19) Venkatesh, M.; Rao, K. S.; Abhilash, T. S.; Tewari, S. P.; Chaudhary, A. K. Optical Characterization of GaAs Photoconductive Antennas for Efficient Generation and Detection of Terahertz Radiation. *Opt. Mater.* **2014**, *36*, 596−601.
(20) Mottamchetty, V.; Chaudhary, A. K. Improvised design of THz spectrophotometer using LT-GaAs photoconductive antennas, pyroelectric detector and band-pass filters. *Indian J. Phys.* **2016**, *90*, 73−78.
(21) Venkatesh, M.; Chaudhary, A. K. Generation of THz radiation from Low temperature Gallium Arsenide (LT-GaAs) photoconductive (PC) antennas using tunable femtosecond oscillator. In *12th International Conference on Fiber Optics and Photonics*, 2014, S5A.33.
(22) Damarla, G.; Venkatesh, M.; Chaudhary, A. K. Temperature-dependent terahertz spectroscopy and refractive index measurements of aqua-soluble and plastic explosives. *Appl. Opt.* **2018**, *57*, 8743−8750.
(23) Trzcinski, T.; Palka, N.; Szustakowski, M. THz Spectroscopy of Explosive-Related Simulants and Oxidizers. *Bull. Polish Acad. Sci. Tech. Sci.* **2011**, *59*, 445−447.
(24) Frisch, M. J.; Trucks, G. W.; Schlegel, H. B.; Scuseria, G. E.; Robb, M. A.; Cheeseman, J. R.; Scalmani, G.; Barone, V.; Mennucci, B.; Petersson, G. A.; et al. *Gaussian09*; Revision D.01; Gaussian Inc.: Wallingford CT, 2010.
(25) Feng, R.; Li, W.; Zhou, Q.; Mu, K.; Zhang, L.; Zhang, C. Terahertz Spectroscopic Investigations of Explosives and the Related Compounds. *Proc. SPIE—Int. Soc. Opt. Eng.*, 2009; Vol. *7158*, pp 1−9.
(26) Hangyo, M.; Nagashima, T.; Nashima, S. Spectroscopy by Pulsed Terahertz Radiation. *Meas. Sci. Technol.* **2002**, *13*, 1727−1738.
(27) (a) Singh, R. P.; Verma, R. D.; Meshri, D. T.; Shreeve, J. n. M. Energetic nitrogen-rich salts and ionic liquids. *Angew. Chem., Int. Ed.* **2006**, *45*, 3584−3601. (b) Steinhauser, G.; Klapötke, T. M. "Green" Pyrotechnics: A Chemists' Challenge. *Angew. Chem., Int. Ed.* **2008**, *47*, 3330−3347. (c) Singh, R. P.; Gao, H.; Meshri, D. T.; Shreeve, J. M. *High Energy Density Materials*; Klapotke, T. M., Ed.; Springer: Berlin, 2007; pp 35−83; (d) Klapötke, T. M. *High Energy Density Materials*; Klapotke, T. M., Ed.; Springer: Berlin, 2007; pp 85−122.
(28) (a) Klapötke, T. M.; Sabaté, C. M. Bistetrazoles: Nitrogen-Rich, High-Performing, Insensitive Energetic Compounds. *Chem. Mater.* **2008**, *20*, 3629−3637. (b) Joo, Y.-H.; Shreeve, J. n. M. High-density energetic mono- or bis(oxy)-5-nitroiminotetrazoles. *Angew. Chem., Int. Ed.* **2010**, *49*, 7320. (c) Stierstorfer, J.; Tarantik, K. R.; Klapötke, T. M. New Energetic Materials: Functionalized 1-Ethyl-5-aminotetrazoles and 1-Ethyl-5-nitriminotetrazoles. *Chem.—Eur. J.* **2009**, *15*, 5775−5792.
(29) Payne, M. C.; Teter, M. P.; Allan, D. C.; Arias, T. A.; Joannopoulos, J. D. Iterative minimization techniques forab initiototal-energy calculations: molecular dynamics and conjugate gradients. *Rev. Mod. Phys.* **1992**, *64*, 1045−1097.
(30) Segall, M. D.; Lindan, P. J. D.; Probert, M. J.; Pickard, C. J.; Hasnip, P. J.; Clark, S. J.; Payne, M. C. First-Principles Simulation: Ideas, Illustrations and the CASTEP Code. *J. Phys. Condens. Matter* **2002**, *14*, 2717−2744.
(31) Fischer, T. H.; Almlof, J. General Methods for Geometry and Wave Function Optimization. *J. Phys. Chem.* **1992**, *96*, 9768.
(32) Vanderbilt, D. Soft Self-Consistent Pseudopotentials in a Generalized Eigenvalue Formalism. *Phys. Rev. B: Condens. Matter Mater. Phys.* **1990**, *41*, 7892−7895.
(33) Monkhorst, H. J.; Pack, J. D. Special points for Brillouin-zone integrations. *Phys. Rev. B: Solid State* **1976**, *13*, 5188−5192.
(34) Perdew, J. P.; Burke, K.; Ernzerhof, M. Generalized Gradient Approximation Made Simple. *Phys. Rev. Lett.* **1996**, *77*, 3865−3868.
(35) Pellizzeri, S.; Delaney, S. P.; Korter, T. M.; Zubieta, J. Using Terahertz Spectroscopy and Solid-State Density Functional Theory to Characterize a New Polymorph of 5-(4-Pyridyl)Tetrazole. *J. Phys. Chem. A* **2014**, *118*, 417−426.
(36) Grimme, S. Semiempirical GGA-Type Density Functional Constructed with a Long-Range Dispersion Correction. *J. Comput. Chem.* **2006**, *27*, 1787.
(37) Kroumova, E.; Aroyo, M. I.; Perez-Mato, J. M.; Kirov, A.; Capillas, C.; Ivantchev, S.; Wondratschek, H. Bilbao Crystallographic Server : Useful Databases and Tools for Phase-Transition Studies. *Phase Transitions* **2003**, *76*, 155−170.
(38) Baroni, S.; de Gironcoli, S.; Giannozzi, P. Phonons and related crystal properties from density-functional perturbation theory. *Rev. Mod. Phys.* **2001**, *73*, 515−562.
(39) Milman, V.; Refson, K.; Clark, S. J.; Pickard, C. J.; Yates, J. R.; Gao, S.-P.; Hasnip, P. J.; Probert, M. I. J.; Perlov, A.; Segall, M. D. Electron and Vibrational Spectroscopies Using DFT, Plane Waves and Pseudopotentials: CASTEP Implementation. *J. Mol. Struct. THEOCHEM* **2010**, *954*, 22−35.
(40) Hamann, D. R.; Schlüter, M.; Chiang, C. Norm-Conserving Pseudopotentials. *Phys. Rev. Lett.* **1979**, *43*, 1494−1497.
(41) Becke, A. D. A new mixing of Hartree-Fock and local density-functional theories. *J. Chem. Phys.* **1993**, *98*, 1372−1377.
(42) Perdew, J. P.; Ernzerhof, M.; Burke, K. Rationale for Mixing Exact Exchange with Density Functional Approximations. *J. Chem. Phys.* **1996**, *105*, 9982−9985.
(43) Dmitriev, V. G.; Gurzadyan, G. G.; Nikogosyan, D. N. *Handbook of Nonlinear Optical Crystals*, 3rd ed.; Springer-Verlag: Berlin Heidelberg, 1999.
(44) Kronik, L.; Neaton, J. B. Excited-State Properties of Molecular Solids from First Principles. *Annu. Rev. Phys. Chem.* **2016**, *67*, 587−616.

DOI: 10.1021/acsomega.8b03383
ACS Omega 2020, 5, 2541−2551

(45) Wu, R. Z.; Fang, Z. X.; Liu, P.; Cao, Q. Z.; Qiu, M.; Li, Y.; Chen, W. K.; Huang, X.; Zhang, Y. F. Electronic Structures and Optical Properties of Organic DAST and DSTMS Crystal Materials. *Acta Phys. Chim. Sinica* **2013**, *29*, 2534.
(46) Zou, G.; Ye, N.; Huang, L.; Lin, X. Alkaline-alkaline earth fluoride carbonate crystals $ABCO_3F$ (A = K, Rb, Cs; B = Ca, Sr, Ba) as nonlinear optical materials. *J. Am. Chem. Soc* **2011**, *133*, 20001−20007.
(47) Narsimha Rao, E.; Appalakondaiah, S.; Yedukondalu, N.; Vaitheeswaran, G. Structural, Electronic and Optical Properties of Novel Carbonate Fluorides $ABCO_3F$ (A=K, Rb, Cs; B=Ca, Sr). *J. Solid State Chem.* **2014**, *212*, 171−179.
(48) Rao, E. N.; Vaitheeswaran, G.; Reshak, A. H.; Auluck, S. Effect of Lead and Caesium on the Mechanical, Vibrational and Thermodynamic Properties of Hexagonal Fluorocarbonates: A Comparative First Principles Study. *RSC Adv.* **2016**, *6*, 99885−99897.
(49) Narsimha Rao, E.; Vaitheeswaran, G.; Reshak, A. H.; Auluck, S. Role of Spin-Orbit Interaction on the Nonlinear Optical Response of $CsPbCO_3F$ Using DFT. *Phys. Chem. Chem. Phys.* **2017**, *19*, 31255−31266.

DOI: 10.1021/acsomega.8b03383
ACS Omega 2020, 5, 2541−2551